NJC

Accepted Manuscript

This article can be cited before page numbers have been issued, to do this please use: M. S. Ghasemzadeh and B. Akhlaghinia, *New J. Chem.*, 2019, DOI: 10.1039/C9NJ00352E.

ROYAL SOCIETY OF CHEMISTRY

rsc.li/njc

ROYAL SOCIETY OF CHEMISTRY
View Article Online
DOI: 10.1039/C9NJ00352E

Journal Name

ARTICLE

C-P bond construction catalyzed by Ni^{II} immobilized on aminated Fe_3O_4@TiO_2 yolk-shell NPs functionalized by (3-glycidyloxypropyl)trimethoxysilane (Fe_3O_4@TiO_2 YS-GLYMO-UNNi^{II}) in green media

Received 00th January 20xx,
Accepted 00th January 20xx

DOI: 10.1039/x0xx00000x

www.rsc.org/

Maryam Sadat Ghasemzadeh [a] and Batool Akhlaghinia,*[a]

Ni^{II} immobilized on aminated Fe_3O_4@TiO_2 yolk-shell NPs functionalized by (3-glycidyloxypropyl)trimethoxysilane (Fe_3O_4@TiO2 YS-GLYMO-UNNi^{II}) was prepared as a stable, highly efficient, and reusable magnetic nanostructured catalyst for the C-P cross coupling reaction. A variety of spectroscopic and microscopic techniques such as Fourier transform infrared (FT-IR) spectroscopy, X-ray diffraction (XRD) analysis, transmission electron microscopy (TEM), field emission scanning electron microscopy (FE-SEM), energy-dispersive X-ray spectroscopy (EDS), EDS-map, thermogravimetric analysis (TGA), vibrating sample magnetometry (VSM), inductively coupled plasma atomic emission spectroscopy (ICP-AES) and CHNS analysis were used to characterize the synthesized nanostructured catalyst. The characterizations determined that the nanostructured catalyst is superparamagnetic in nature, structured as core-shell and its average particle size is 30-32 nm. The catalytic activity of this new magnetic nanostructured catalyst (Fe_3O_4@TiO_2 YS-GLYMO-UNNi^{II}) was examined in the C-P cross coupling reaction of aryl halides/ aryl boronic acids/ styrene/ phenylacetylene with diethylphosphite/ triethylphosphite in the presence of WERSA so that arylphosphonates/ vinylphosphonate/ alkynylphosphonate could be prepared in a short period of time. In all the cases, the nanostructured catalyst could be easily recovered magnetically for at least seven runs and a simple work-up procedure was used to isolate the obtained products. The present methodology proved to be quite suitable for scale-up and commercialization.

1. Introduction

Among the plethora of organic compounds, organophosphorus compounds occupy a significant position. Over the recent decades, much attention has been paid to research dedicated to the development of versatile methods for the synthesis of organophosphorous compounds[1-3] owing to their widespread applications in medicinal chemistry,[4-6] materials chemistry,[7,8] organic synthesis[9,10] and catalysis.[11,12] The transition metal (including Ni, Cu, Mn, Rh, Ag, Zn, Zr, Fe and Pd) catalyzed carbon-phosphorus (C-P) bond-forming reactions between C_{sp2}-X, $B(OH)_2$, H/or C_{sp}-H and diethylphosphite /or triethylphosphite are the first powerful, reliable and the most widely-used methods for the synthesis of various types of organophosphorus compounds.[13-40] Based on the ideology of green chemistry, much attention has been concentrated on the development of these classic methods *via* the modification and improvement of the catalyst,[41,42] and reaction conditions[38,40] to meet the requirements of contemporary synthetic organic demands which calls energy efficiency, operational simplicity and environmental safety. Nevertheless, despite the fact that the reported traditional synthetic entries into carbon-phosphorus (C-P) bond-forming reactions are suitable, some of them still have limitations and suffer from severe problems related to the separation, recovery, and instability of the homogeneous catalysts (result in undesirable metal contamination of the products) as well as use of volatile and hazardous organic solvents,[31,39,43] the requirement of expensive ligands,[44,45] aggressive reagents (caused a lack of tolerance for functional groups), microwave oven[33] and long reaction times to give good conversions. Therefore, effort to elaborate a new catalytic method of industrial applicability with (a) insensitivity to air, (b) recyclability, (c) sustainability from an environmental point of view, (d) versatility, and (e) potential scalability for the easy preparation of organophosphorus compounds *via* direct C-P bond forming reactions could be the subject of intense research in this area.[46-55] With respect to the principle of green chemistry in organic synthesis, heterogenization of homogeneous catalyst through the immobilization of homogeneous catalyst on a suitable insoluble supporting material enables efficient removal and recycling of the catalyst and minimizes the amount of waste as well. In addition, magnetic nanoparticles (MNPs) are being applied as attractive solid supports for the immobilization of homogeneous catalysts due to their simple handling, low cost, super magnetic susceptibility, easy recovery with an external magnetic field, high catalytic activity and high stability in various organic transformations.[56]

[a]*Department of Chemistry, Faculty of Science, Ferdowsi University of Mashhad, Mashhad 9177948974, Iran. E-mail: akhlaghinia@um.ac.ir; Fax: +98-51-3879-5457; Tel: +98-51-3880-5527*

Electronic Supplementary Information (ESI) available: General information, and spectral data of organic compounds. See DOI: 10.1039/x0xx00000x

Moreover, Fe_3O_4 NPs have drawn the most attention owing to their strong magnetic responsiveness, low toxicity, excellent stability, biocompatibility, large surface-to-volume ratio and their potential applications.[57,58] The magnetite NPs tend to aggregate due to anisotropic dipolar attraction, and thereby lose their catalytic activity and dispersibility. These problems can be untangled by coating with a sustainable layer such as polymer,[59] metal oxide (MO),[60] carbon[61] and silica,[62] as the stabilizer, to form a core-shell and/or yolk-shell structures. Yolk-shell nanostructures (YSNPs) have diverse applications including catalysis,[63] microwave absorber,[64] sensors[65] and biomedicine.[66] However, YSNPs have drawn significant attention in recent years because of their unique properties such as low density, large surface area and ease of interior core functionalization in spite of core-shell structures.[67] Metal-organic frameworks (MOFs) have been the focus of increasing attention during the past decade.[68] MOF-based structures show several advantages such as high surface areas, adjustable pore sizes, and the simplicity of processability.[69,70] In addition, MOFs and functionalized- or modified-MOFs have been applied as solid catalysts in Sonogashira,[71] alkene epoxidation,[72] Knoevenagel,[73,74] Friedel-Crafts alkylation and acylation,[75] Suzuki,[76] Biginelli[77] and aza-Michael reactions.[78]Considering the importance of developing a new procedure using a heterogeneous nanocatalyst for the C-P bond formation, and in continuation of our recent studies on the introduction of sustainable chemistry and heterogeneous nanocatalyst,[79-100] herein, Ni^{II} immobilized on aminated $Fe_3O_4@TiO_2$ yolk-shell NPs functionalized by (3-glycidyloxypropyl)trimethoxysilane ($Fe_3O_4@TiO_2$ YS-GLYMO-UNNi^{II}) was synthesized according the synthetic process illustrated in Scheme 1. In this line, functionalization of $Fe_3O_4@TiO_2$ YSNPs was carried out by (3-glycidyloxypropyl)trimethoxysilane and further reaction with UiO-66(Zr)-NH_2 (**V'**) to produce aminated $Fe_3O_4@TiO_2$ yolk-shell NPs. Then, immobilization of Ni^{II} was performed *via* a reaction of $Fe_3O_4@TiO_2$ YS-GLYMO-UN with ethanolic solution of $Ni(OAc)_2.4H_2O$. Afterwards, the catalytic activity of $Fe_3O_4@TiO_2$ YS-GLYMO-UNNi^{II} (**VII**) was subsequently investigated toward the C-P cross coupling reaction, in green media (see Scheme 2).

2. Experimental

2.1. General

All chemical reagents and solvents were purchased from Merck and Sigma-Aldrich chemical companies and were used as received without further purification. The purity determinations of the products were accomplished by TLC on silica gel polygram STL G/UV 254 plates. The melting points of the products were determined with an Electrothermal Type 9100 melting point apparatus. The FT-IR spectra were recorded on an Avatar 370 FT-IR Therma Nicolet spectrometer. Elemental analyses were performed using a Thermo Finnegan Flash EA 1112 Series instrument. The NMR spectra were obtained in Brucker Avance 300 and 400 MHz instruments in $CDCl_3$. Mass spectra were recorded with a CH7A Varianmat Bremem instrument at 70 eV electron impact ionization, in m/z (rel %). The crystal structure of catalyst was analyzed by XRD using Model PW1730 (manufactured in the Netherlands) diffractometer Dectvis operated at 40 kV and 30 mA utilizing Cu Kα radiation (λ= 0.15056 A°). Transmission electron microscopy (TEM) was performed with a Zeiss-EM10C (manufactured in Germany) with an accelerating voltage of 100 KV. FE-SEM images, EDS and EDS-map were recorded using a TESCAN, Model: MIRA3 scanning electron microscope operating at an acceleration voltage of 30.0 kV and resolution of about 200 and 500 nm (manufactured in the Czech Republic). TGA analysis was carried out on a Shimadzu Thermogravimetric Analyzer (TG-50) in the temperature range of 25-900 °C at a heating rate of 10 °C min^{-1} under air atmosphere. The magnetic properties of the catalyst were measured using a vibrating sample magnetometer (VSM, Magnetic Danesh Pajoh Inst.). Inductively coupled plasma atomic emission spectroscopy (ICP-AES) was carried out with a Varian VISTA-PRO, CCD (Australia). All yields refer to isolated products after purification by thin layer chromatography.

2.2. Preparation of magnetite nanoparticles Fe_3O_4 NPs (I)

Under Ar atmosphere at room temperature, $FeCl_2.4H_2O$ (10 mmol, 1.99 g) and $FeCl_3.6H_2O$ (12 mmol, 3.25 g) were dissolved in deionized water (30 mL). Subsequently, to the stirring mixture, NH_4OH solution (0.6 M, 200 mL) was then added dropwise to reach the reaction pH of 11. The resulting black dispersion was continuously stirred for 1 h at room temperature, and then refluxed for 1 h. The magnetic nanoparticles were separated with a magnetic field and washed with deionized water until it was neutralized. Fe_3O_4 NPs (**I**) was then dried at 50 °C for 24 h.

2.3. Preparation of $Fe_3O_4@SiO_2$ (II) core-shell

The as-prepared Fe_3O_4 NPs (**I**) (3.5 g) were dispersed in a mixture of ethanol (160 mL), water (40 mL), and NH_4OH (0.6 M, 3.5 mL). Subsequently, TEOS (0.009 mmol, 2.0 mL) was added dropwise, and the reaction was allowed to proceed for 24 h under stirring at 40 °C. The resulting $Fe_3O_4@SiO_2$ (**II**) was washed with ethanol, separated by magnetic decantation and dried at 60 °C for 12 h under vacuum.

2.4. Preparation of $Fe_3O_4@SiO_2@TiO_2$ (III)

The obtained $Fe_3O_4@SiO_2$ (**II**) (3 g) were first calcined at 300 °C in static air for 2 h and then dispersed in isopropyl alcohol (41.47 mL), followed by the addition of NH_4OH (0.6 M, 3.0 mL). After stirring for 5 min, tetra-n-butyl orthotitanate (TNBT) (5.8 mmol, 2 g) was added to the reaction mixture. The resulting mixture was then transferred into a Teflon-lined stainless steel autoclave with a capacity of 100 mL and kept at 200 °C for 24 h to obtain $Fe_3O_4@SiO_2@TiO_2$ (**III**).[101]

2.5. Preparation of $Fe_3O_4@TiO_2$ (IV) yolk-shell

$Fe_3O_4@SiO_2@TiO_2$ (**III**) (2 g) was mixed with an aqueous solution of KOH (0.2 M, 40 mL) that was heated in a water bath at 50 °C for 24 h. The resulting mixture was washed with ethanol (4× 20) and dried at 60 °C under vacuum overnight. Finally, the powder was calcined at 400 °C under Ar atmosphere for 2 h with a heating rate of 5 °C min^{-1} to obtain the $Fe_3O_4@TiO_2$ (**IV**) yolk-shell.[101]

2.6. Preparation of $Fe_3O_4@TiO_2$ YS-GLYMO (V)

$Fe_3O_4@TiO_2$ (**IV**) (2.0 g) was dispersed in dry toluene (40 mL) by sonication for 1 h. Next, (3-glycidyloxypropyl)trimethoxysilane (GLYMO) (4.5 mmol, 1 mL) was added to the resulting mixture and slowly heated to reflux for 24 h. The obtained $Fe_3O_4@TiO_2$ YS-GLYMO (**V**) was separated by an external magnet and washed in turn by diethyl ether (2× 30 mL), CH_2Cl_2 (3× 30 mL) and dried at 80 °C

for 12 h under vacuum. Elemental analysis and TGA showed that the loading amount of C atom was 0.4 mmol per gram of catalyst.

2.7. Preparation of UiO-66(Zr)-NH_2 (V')

$ZrCl_4$ (1.0 mmol, 0.23 g) and 2-aminoterephthalic acid (H_2ATA) (1.0 mmol, 0.18 g) were dissolved in DMF (50 mL), and then the solution was transferred to a 100 mL Teflon-lined stainless steel autoclave. The autoclave was sealed and heated in an oven at 120 °C for 48 h. The mixture was washed with methanol (4×15) to eliminate the occluded DMF. The UiO-66(Zr)-NH_2 (**V'**) was obtained by drying under vacuum at 100 °C for 24 h.[102]

View Article Online
DOI: 10.1039/C9NJ00352E

Journal Name

ARTICLE

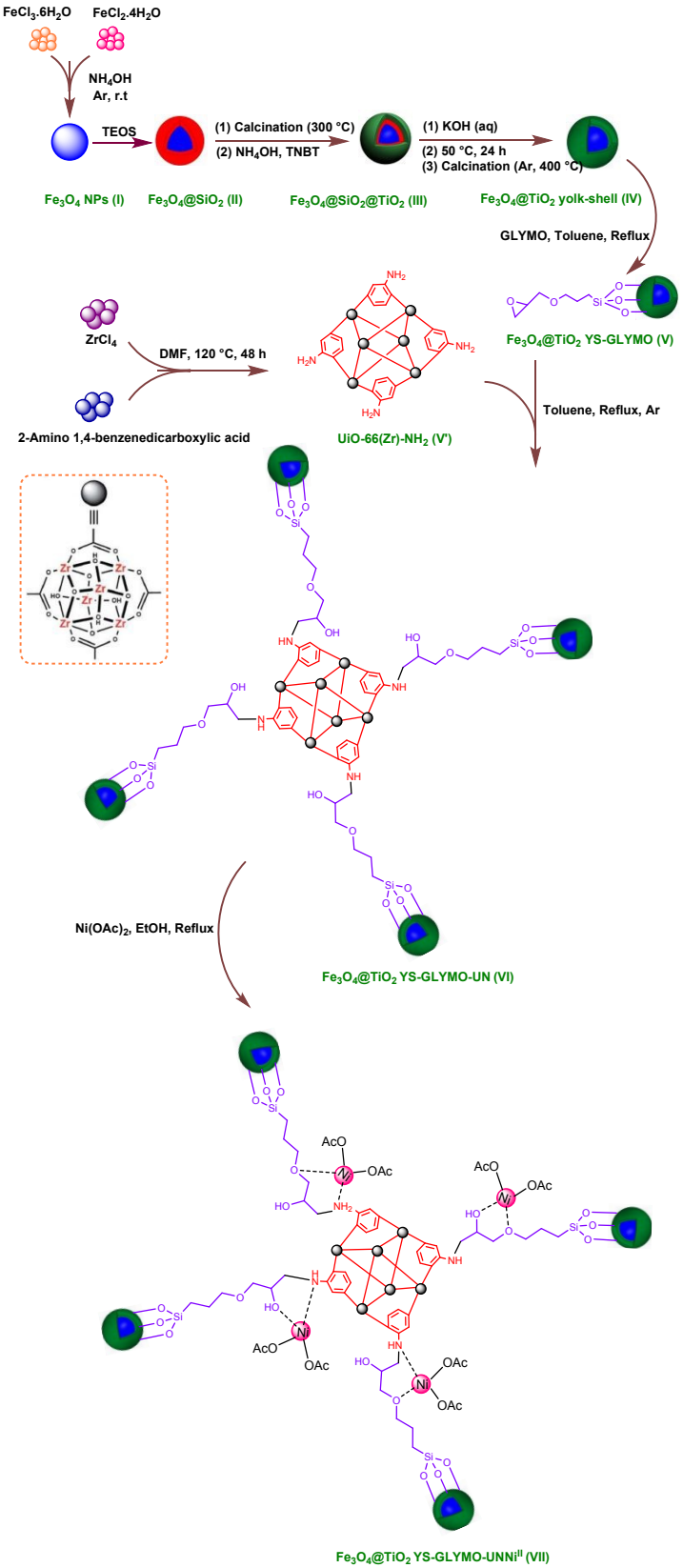

Scheme 1 Preparation of Ni^{II} immobilized on aminated Fe_3O_4@TiO_2 yolk-shell NPs functionalized by (3-glycidyloxypropyl)trimethoxysilane (Fe_3O_4@TiO_2 YS-GLYMO-UNNi^{II} (**VII**)).

View Article Online
DOI: 10.1039/C9NJ00352E

2.8. Preparation of Fe_3O_4@TiO_2 YS-GLYMO-UN (VI)

The prepared Fe_3O_4@TiO_2 YS-GLYMO (**V**) (1.5 g) was sonicated in dry toluene (50 mL) for 1 h. Then, UiO-66(Zr)-NH_2 (**V'**) (0.7 g) was added to the dispersed Fe_3O_4@TiO_2 YS-GLYMO (**V**) in toluene under Ar atmosphere and stirred under reflux conditions for 24 h. The resulting Fe_3O_4@TiO_2 YS-GLYMO-UN (**VI**) was separated by an external magnet and washed with dry toluene (4× 25) and dried at 80 °C for 24 h under vacuum. Elemental analysis and TGA showed that the loading amount of N atom was 0.58 mmol per gram of catalyst.

2.9. Preparation of Fe_3O_4@TiO_2 YS-GLYMO-UNNi^{II} (VII)

To a solution of $Ni(OAc)_2.4H_2O$ (6 mmol, 1.48 g) in dry ethanol (50 mL), the obtained Fe_3O_4@TiO_2 YS-GLYMO-UN (**VI**) (2 g) was added and refluxed for 24 h. The resulting Fe_3O_4@TiO_2 YS-GLYMO-UNNi^{II} (**VII**) was separated with an external magnet and washed with ethanol (3 × 30 mL) before drying at 60 °C under vacuum (24h).

2.10. Typical procedure for the preparation of diethyl phenylphosphonate in the presence of Fe_3O_4@TiO_2 YS-GLYMO-UNNi^{II} (VII)

Fe_3O_4@TiO_2 YS-GLYMO-UNNi^{II} (0.4 mol%, 0.3 g) was added to a stirring solution of iodobenzene (1.0 mmol, 0.203 g), diethylphosphite (2.1 mmol, 0.28 g)/or triethylphosphite (2.1 mmol, 0.34 g) and water extract of rice straw ash (WERSA) (2.5 mL) at 90 °C. After completion of the reaction (2.10/1.15 h) which was monitored by TLC, the reaction mixture was cooled to room temperature. The catalyst was separated by a magnetic field, washed with EtOAc (3 × 20 mL), dried and reused for a consecutive run under the same reaction conditions. The reaction mixture was then extracted with ethyl acetate (3 × 15 mL) and the combined organic layer was dried over anhydrous Na_2SO_4. After evaporation of the solvent, the crude product was purified by thin layer chromatography using ethylacetate/ methanol (10 : 3) to afford the pure diethyl phenylphosphonate (0.140 g, 95% yield).

2.11. Preparation of water extract of rice straw ash (WERSA)

Dried rice straws were burnt to ashes to prepare the water extract of rice straw ash (WERSA). 5 g of the ash was suspended in deionized water (50 mL) and stirred for 30 min at room temperature. The mixture was then filtered and the filtrate was used as WERSA. WERSA consists of SiO_2 (74.31 %), $A1_2O_3$ (1.40 %), Fe_2O_3 (0.73 %), TiO_2 (0.02%), CaO (1.61 %), MgO (1.89 %), K_2O (11.30 %), Na_2O (1.85 %) and P_2O_5 (2.65%). Finally, litmus test was used to determine the pH of WERSA and it was found to be 12.[103]

2.12. Spectral data

Diethyl phenylphosphonate (1a).[35] Oil; isolated yield: 95%; ^{1}H NMR: δH (400 MHz; $CDCl_3$; Me_4Si) 1.32-1.29 (t, *JH,H*= 6.8 Hz, 6 H), 4.16-4.05 (m, 4 H), 7.47-7.42 (m, 2 H), 7.53-7.51 (m, 1 H), 7.80 (dd, *JH,H*= 13.2, *JH,H*= 8.4, 2 H); ^{13}C NMR: δC (100 MHz; $CDCl_3$; Me_4Si) 16.3 (d, *JCP*= 7.0 Hz), 62.0 (d, *JCP*= 5.0 Hz), 131.7 (d, *JCP*= 10.0 Hz), 128.3 (d, *JCP*= 186.0 Hz), 128.4 (d, *JCP*= 15.0 Hz), 132.3 (d, *JCP*= 3.0 Hz); MS, *m/z* 214 (M^+, 5%).

Diethyl (4-methoxyphenyl)phosphonate (1d).[35] Oil; isolated yield: 90%; ^{1}H NMR: δH (400 MHz; $CDCl_3$; Me_4Si) 1.29-1.25 (t, *JHH*= 7.2 Hz, 6 H), 3.80 (s, 3 H), 4.09-3.97 (m, 4 H), 6.93 (dd, *JHH*= 8.8 Hz, *JHH*= 3.2 Hz, 2 H), 7.71 (dd, *JHH*= 12.8 Hz, *JHH*= 8.8 Hz, 2 H); ^{13}C NMR: δC (100 MHz, $CDCl_3$) 16.2 (d, *JCP*= 6.0 Hz), 55.2, 61.8 (d, *JCP*= 6.0 Hz), 113.9 (d, *JCP*= 16.0 Hz), 119.3 (d, *JCP*= 193.0 Hz), 133.7 (d, *JCP*= 12.0 Hz), 162.8 (d, *JCP*= 4.0 Hz); MS, *m/z* 244 (M^+, 8%).

Diethyl *p*-tolylphosphonate (1e).[35] Oil; isolated yield: 90%; ^{1}H NMR: δH (300 MHz; $CDCl_3$; Me_4Si) 1.35-1.31 (t, *J*HH= 6.9 Hz, 6H), 2.42 (s, 3H), 4.21-4.01 (m, 4H), 7.29 (dd, *JHH*= 8.1 Hz, *JHH*= 3.3 Hz, 2H), 7.72 (dd, *JHH*= 13.2 Hz, *JHH*= 8.1 Hz, 2H); ^{13}C NMR: δC (75 MHz; $CDCl_3$; Me_4Si) 16.1 (d, *JCP*= 6.7 Hz), 16.3 (d, *JCP*= 6.7 Hz), 21.6, 61.9 (d, *JCP*= 5.2 Hz), 124.9 (d, *JCP*= 188.2 Hz), 129.2 (d, *JCP*= 15.0 Hz), 131.8 (d, *JCP*= 9.7 Hz), 142.9 (d, *JCP*= 3.0 Hz); MS, *m/z* 228 (M^+, 5%).

Diethyl (4-nitrophenyl)phosphonate (1h). [35] Oil; isolated yield: 90%; ^{1}H NMR: δH (300 MHz; $CDCl_3$; Me_4Si) 1.36-1.32 (t, *JHH*= 6.9 Hz, 6H), 4.27-4.06 (m, 4H), 8.00 (dd, *JHH*= 12.7 Hz, *JHH* = 8.7 Hz, 1H), 8.3(dd, *JHH*= 8.7 Hz, *JHH* = 3.3 Hz, 1H); ^{13}C NMR: δC (75 MHz; $CDCl_3$; Me_4Si) 16.1 (d, *JCP*= 6.7 Hz), 16.3 (d, *JCP*= 6.0 Hz), 62.7 (d, *JCP*= 5.2 Hz), 123.3 (d, *JCP*= 15.0 Hz), 133.0 (d, *JCP*= 10.5 Hz), 135.8 (d, *JCP*=185.2 Hz), 150.2 (d, *JCP*= 3.7 Hz); MS, *m/z* 257 (M^+, 6%).

3. Results and discussion

3.1. The characterization of Fe_3O_4@TiO_2 YS-GLYMO-UNNi^{II} (VII)

The novel magnetic nanostructured catalyst denoted as Fe_3O_4@TiO_2 YS-GLYMO-UNNi^{II} (**VII**) was prepared *via* stepwise procedure according to Scheme 1. The Fe_3O_4 MNPs were prepared by coprecipitation of Fe (III) and Fe (II) salts in the presence of NH_4OH solution under Ar atmosphere at room temperature. Next, Fe_3O_4 NPs (**I**) was coated with a layer of silica through stirring Fe_3O_4 NPs (**I**) suspension in ethanol/ deionized water with tetraethyl orthosilicate. The as-prepared Fe_3O_4@SiO_2 (**II**) core-shell was first calcined in static air, followed by addition of NH_4OH and tetra-n-butyl orthotitanate to achieve Fe_3O_4@SiO_2@TiO_2 (**III**). The obtained Fe_3O_4@SiO_2@TiO_2 (**III**) was treated with KOH (aq) and then calcinated under Ar atmosphere to produce Fe_3O_4@TiO_2 (**IV**) yolk-shell. After preparing the Fe_3O_4@TiO_2 (**IV**) yolk-shell, the obtained nanoparticles were subsequently reacted with (3-glycidyloxypropyl)trimethoxysilane and then UiO-66(Zr)-NH_2 (**V'**) to form Fe_3O_4@TiO_2 YS-GLYMO-UN (**VI**). Finally, Ni^{II} was immobilized on the surface of Fe_3O_4@TiO_2 YS-GLYMO-UN (**VI**) through the reaction of Fe_3O_4@TiO_2 YS-GLYMO-UN (**VI**) with ethanolic solution of $Ni(OAc)_2.4H_2O$ under reflux.

Characterization of Ni^{II} immobilized on aminated Fe_3O_4@TiO_2 yolk-shell NPs functionalized by 3-glycidyloxypropyl)trimethoxysilane (Fe_3O_4@TiO_2 YS-GLYMO-UNNi^{II} (**VII**)) was studied using some microscopic and spectroscopic techniques including Fourier transform infrared (FT-IR) spectroscopy, X-ray diffraction analysis (XRD), transmission electron microscopy (TEM), field emission scanning electron microscopy (FE-SEM), energy-dispersive X-ray (EDS), EDS-map, thermogravimetric analysis (TGA), vibrating sample magnetometry (VSM), inductively coupled plasma atomic emission spectroscopy (ICP-AES) and elemental analysis (CHNS) analysis.

FT-IR spectroscopy was used to confirm the presence of corresponding functional groups at different steps involved in the preparation of the nanostructured catalyst (Scheme 1). Figure 1 demonstrates the FT-IR spectra of (a) $Fe_3O_4@SiO_2$ (**II**), (b) $Fe_3O_4@SiO_2@TiO_2$ (**III**), (c) $Fe_3O_4@TiO_2$ yolk-shell (**IV**), (d) $Fe_3O_4@TiO_2$ YS-GLYMO (**V**), (e) UiO-66(Zr)-NH_2 (**V'**), (f) $Fe_3O_4@TiO_2$ YS-GLYMO-UN (**VI**), (g) $Fe_3O_4@TiO_2$ YS-GLYMO-UNNi^{II} (**VII**). As it is evident in Figure 1a, the broad absorption band around 586 cm^{-1} can be attributed to Fe-O vibration. In addition, two broad absorption bands around 3400 and 1084 cm^{-1} can be ascribed to the hydroxyl groups (*v* OH) and Si-O-Si bond in $Fe_3O_4@SiO_2$ core-shell (**II**), respectively.

The characteristic band in the region 800-500 cm^{-1} is related to the stretching vibration mode of Ti-O which covered the broad absorption band of Fe-O at 641-575 cm^{-1}. In addition, the stretching vibration of Si-O-Si bond in $Fe_3O_4@SiO_2@TiO_2$ (**III**) can be observed as a strong broad band at 1078 cm^{-1} (Figure 1b). Figure 1c displays the absorption band at 800-579 cm^{-1} allocates the stretching vibration of Ti-O, moreover, the stretching vibrational mode of Si-O-Si was eliminated. Grafting of (3-glycidyloxypropyl)trimethoxysilane on the surface of $Fe_3O_4@TiO_2$ (**IV**) yolk-shell NPs is confirmed by the presence of a typical band at 2929 and 2871 cm^{-1} that are attributed to stretching vibrations of alkyl chains (C-H), and also the characteristic stretching vibration of Si-O bond appears at 1102 (Figure 1d). FT-IR spectrum of UiO-66(Zr)-NH_2 (**V'**) represents the asymmetric and symmetric N-H stretching modes at 3469, 3362 cm^{-1}, also the stretching vibration at 1257 cm^{-1} shows C_{Ar}-N bond.[104] Additionally, the appearance of absorption band at 1657 cm^{-1} attributes to C=O of -COOH groups which coordinated with Zr^{4+}.[104] Besides, the stretching vibration band of C=C bond (aromatic rings), the asymmetric and symmetric stretching modes of the -COO appear at 1570, 1436 and 1387 cm^{-1}, respectively (Figure 1e).[104] Correspondingly, as can be clearly observed in Figure 1e, the strong absorption band at 768 cm^{-1} is related to the stretching vibrations of the Zr-O group in $Zr_6O_4(OH)_4$.[104] Increasing the intensity and frequency of the hydroxyl groups in the FT-IR spectrum shows the successful ring opening of epoxy ring which was performed by UiO-66(Zr)-NH_2 (**V'**) (Figure 1f). Upon Ni^{II} coordination, the intensities of absorption bands of N-H, C_{Ar}-N and Zr-O stretching vibrations are decreased (Figure 1g). *(See supporting information file)*

The crystallographic structures of (a) $Fe_3O_4@TiO_2$ yolk-shell (**IV**), (b) UiO-66(Zr)-NH_2 (**V'**), (c) $Fe_3O_4@TiO_2$ YS-GLYMO-UNNi^{II} (**VII**) and (d) the 7th recovered $Fe_3O_4@TiO_2$ YS-GLYMO-UNNi^{II} (**VII**) from the C-P cross-coupling reaction are investigated by the XRD technique. As is evident in Figure 2a, the XRD pattern shows reflection peaks at 2Θ = 30.1°, 35.5°, 37°, 62.8° and 75° which can be indexed to (2 1 1), (1 1 2), (2 2 0), (0 0 4) and (6 2 0) reflections of the orthorhombic structure of Fe_3O_4, respectively (Ref. Code: 98-001-7122). Additionally, as can be recognized from the XRD pattern of $Fe_3O_4@TiO_2$ yolk-shell (**IV**), the reflection peaks at 2Θ = 25.2°, 38.5°, 47.9°, 53.8°, 54.9°, 62°, 68.7° and 70.1° are related to (1 1 0), (2 1 1), (0 2 0), (5 1 0), (1 2 1), (3 2 1), (6 1 1) and (0 2 2) reflections of the tetragonal structure of TiO_2, respectively (Ref. Code: 98-010-9333). Similarly, the XRD profile of Figure 2b displays that diffraction peaks at 2Θ = 7.34°, 8.48°, 12°, 14°, 17°, 18°, 22°, 25°, 31.5°, 35.5° and 37.5° represent the (1 1 0), (2 0 0), (3 1 1), (2 2 2), (4 0 0), (4 2 0), (5 1 1), (6 0 0), (6 4 0), (8 2 0) and (6 6 2) planes of UiO-66(Zr)-NH_2 (**V'**) structure. However, the structure of UiO-66(Zr)-NH_2 (**V'**) consists of an inner $Zr_6O_4(OH)_4$ core where the triangular faces of the Zr_6-octahedron are alternatively capped by μ_3-O and μ_3-OH groups (Ref. Code: 04-005-5596).[105] Furthermore, the average crystalline size of $Fe_3O_4@TiO_2$ YS-GLYMO-UNNi^{II} (**VII**) which was calculated using Debye-Scherrer equation ($d = K\lambda/(\beta\cos\theta)$) was estimated to be around 31 nm.

Transmission electron microscopy (TEM) was used to determine the size and morphology of $Fe_3O_4@TiO_2$ YS-GLYMO-UNNi^{II} (**VII**) as illustrated in (Figure 3). The morphology of the prepared nanoparticles is shown to be spherical in shape and structured as core-shell. In addition, the size of particles is also about 30-32 nm. Distribution histogram of $Fe_3O_4@TiO_2$ YS-GLYMO-UNNi^{II} (**VII**) also revealed that the average diameter of nanoparticles is 30.9 nm, which corresponds closely with XRD results.

Field emission scanning electron microscopy (FE-SEM) technique was used to illustrate the size and morphology of $Fe_3O_4@TiO_2$ yolk-shell (**IV**) and $Fe_3O_4@TiO_2$ YS-GLYMO-UNNi^{II} (**VII**). As it is evident in Figure 4, FE-SEM images of $Fe_3O_4@TiO_2$ yolk-shell (**IV**) and $Fe_3O_4@TiO_2$ YS-GLYMO-UNNi^{II} (**VII**) reveal that the nanoparticles have spherical shapes with an average particle size of about 887[101] and 31 nm, respectively.

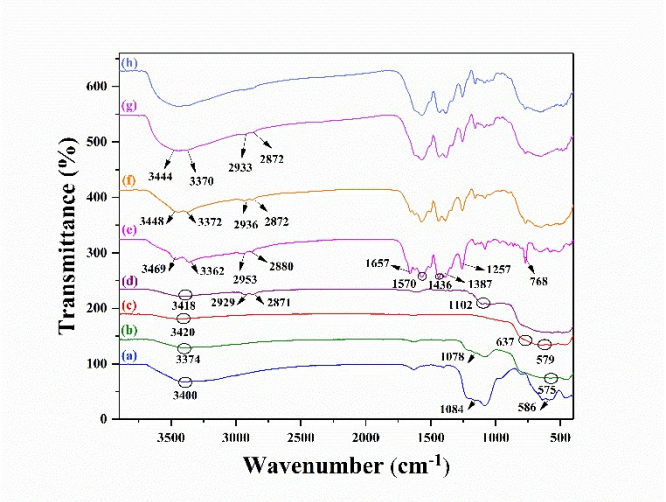

Fig. 1 FT-IR spectra of (a) $Fe_3O_4@SiO_2$ (**II**), (b) $Fe_3O_4@SiO_2@TiO_2$ (**III**), (c) $Fe_3O_4@TiO_2$ yolk-shell (**IV**), (d) $Fe_3O_4@TiO_2$ YS-GLYMO (**V**), (e) UiO-66(Zr)-NH_2 (**V'**), (f) $Fe_3O_4@TiO_2$ YS-GLYMO-UN (**VI**), (g) $Fe_3O_4@TiO_2$ YS-GLYMO-UNNi^{II} (**VII**) and (h) the 7th recovered $Fe_3O_4@TiO_2$ YS-GLYMO-UNNi^{II} (**VII**) from the C-P cross-coupling reaction.

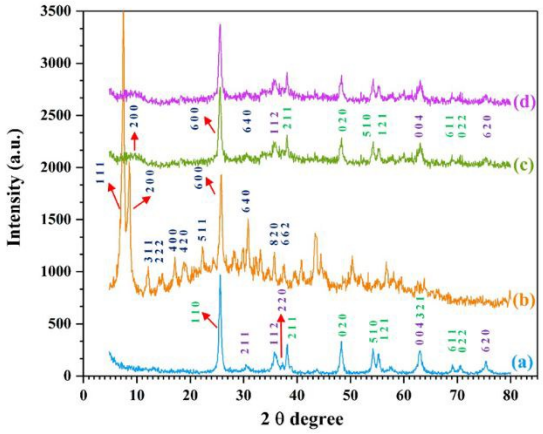

Fig. 2 XRD patterns of (a) Fe_3O_4@TiO_2 yolk-shell (**IV**), (b) UiO-66(Zr)-NH_2 (**V'**), (c) Fe_3O_4@TiO_2 YS-GLYMO-UNNi^{II} (**VII**) and (d) the 7th recovered Fe_3O_4@TiO_2 YS-GLYMO-UNNi^{II} (**VII**) from the C-P cross-coupling reaction.

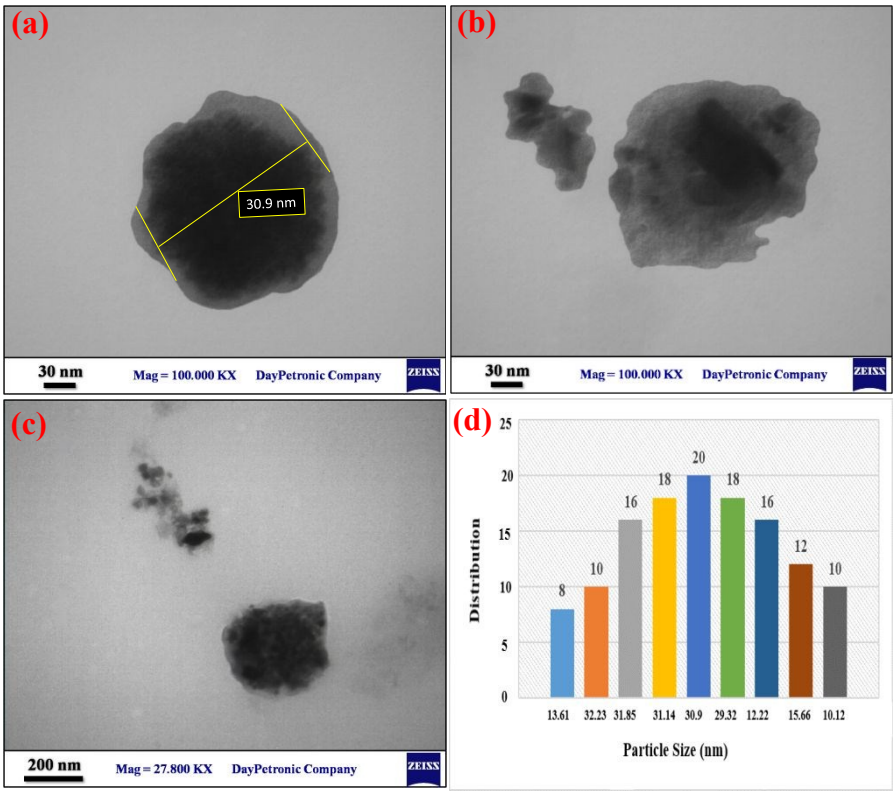

Fig. 3 (a, b, c) TEM images and (d) particle size distribution histogram of Fe_3O_4@TiO_2 YS-GLYMO-UNNi^{II} (**VII**).

View Article Online
DOI: 10.1039/C9NJ00352E

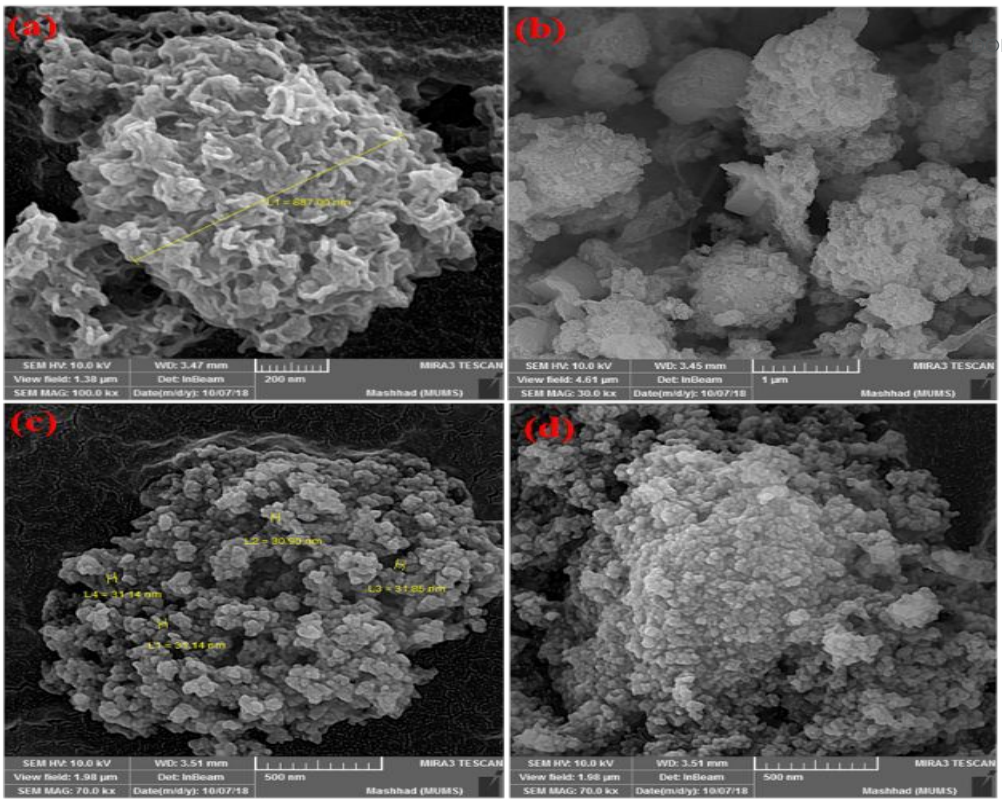

Fig. 4 The FE-SEM images of (a, b) Fe_3O_4@TiO_2 yolk-shell (**IV**) and (c, d) Fe_3O_4@TiO_2 YS-GLYMO-UNNi^{II} (**VII**).

The type of elements in Fe_3O_4@TiO_2 YS-GLYMO-UNNi^{II} (**VII**) was investigated by recording the energy-dispersive X-ray (EDS) spectrum (Figure 5). The presence of Ni, Fe, Ti, Zr, Si, O, N, and C in the EDS spectrum confirmed the composition of the as-synthesized nanostructured catalyst (Fe_3O_4@TiO_2 YS-GLYMO-UNNi^{II} (**VII**)).

The uniform dispersal of Ni, Fe, Ti, Zr, Si, O, N, and C on the surface of nanostructured catalyst is shown by the corresponding EDS-map images of Fe_3O_4@TiO_2 YS-GLYMO-UNNi^{II} (**VII**) (Figure 6).

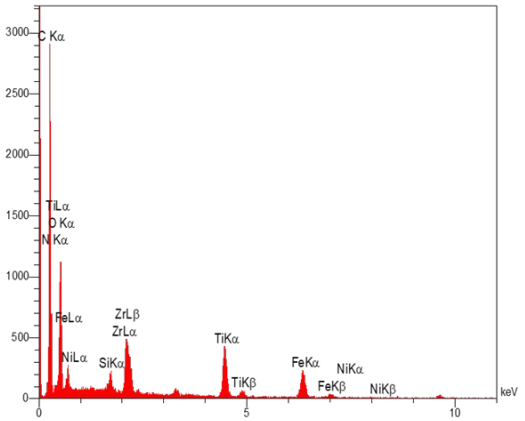

Fig. 5 The EDS analysis of Fe_3O_4@TiO_2 YS-GLYMO-UNNi^{II} (**VII**).

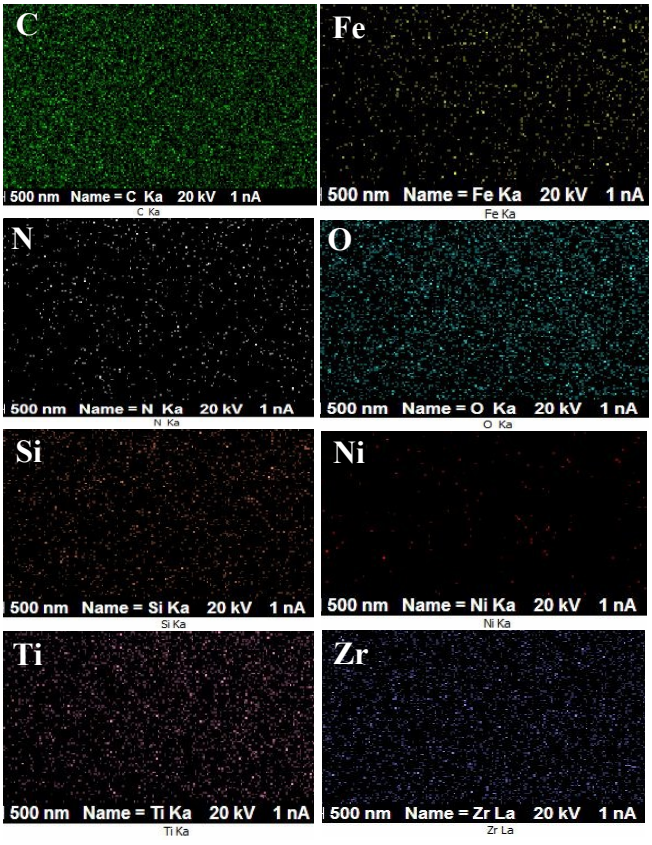

Fig. 6 EDS-map images of Fe_3O_4@TiO_2 YS-GLYMO-UNNi^{II} (**VII**).

View Article Online
DOI: 10.1039/C9NJ00355E

To investigate the thermal stability of (a) Fe_3O_4@TiO_2 yolk-shell (**IV**), (b) Fe_3O_4@TiO_2 YS-GLYMO (**V**), (c) Fe_3O_4@TiO_2 YS-GLYMO-UN (**VI**), (d) Fe_3O_4@TiO_2 YS-GLYMO-UNNi^{II} (**VII**) and the 7th recovered Fe_3O_4@TiO_2 YS-GLYMO-UNNi^{II} (**VII**), TGA analysis was performed under air atmosphere at a heating rate of 10 °C min^{-1} from 25 to 900 °C (Figure 7). The TGA of the Fe_3O_4@TiO_2 yolk-shell (**IV**) (Figure 7a) depicts a rather negligible weight loss (2 %) from 100 to 180 °C verifies water evaporation. Figure 7b demonstrates two steps of weight loss in TGA thermogram of Fe_3O_4@TiO_2 YS-GLYMO (**V**). The first step (150-220 °C, 5 %) corresponds to the loss of physically adsorbed water on the surface of Fe_3O_4@TiO_2 yolk-shell (**IV**). The second step (230-420 °C, 4.8%) is due to the loss of the (3-glycidyloxypropyl)trimethoxysilane linker. Therefore 0.44 mmol/g of organic segments is grafted on the surface of Fe_3O_4@TiO_2 yolk-shell (**IV**). In addition, according to the elemental analysis data, the loading amount of organic segments supported on Fe_3O_4@TiO_2 yolk-shell (**IV**) was 0.4 mmol/g based on carbon content (C= 14.90 %).

TGA thermogram of Fe_3O_4@TiO_2 YS-GLYMO-UN (**VI**) revealed two significant mass changes at different temperature ranges. The first mass change of about 12 %, from 100 to 200 °C, could be assigned to remove of the trapped physically adsorbed water. The second and indeed the significant mass change, which was started at around 210 to 550 °C can be attributed to the elimination of organic functional groups attached on the surface of Fe_3O_4@TiO_2 yolk-shell (**IV**) (24 %). According to the results obtained from the TGA thermogram (Figure 7c), the amount of organic linkers anchored on Fe_3O_4@TiO_2 yolk-shell (**IV**) was estimated to be 0.591 mmol/g. These results were also in good agreement with the obtained elemental analysis data (C= 16.90 %, N= 17.37). In the profile of Fe_3O_4@TiO_2 YS-GLYMO- UN (**VI**), the TGA thermogram (Figure 7c) depicted three-step thermal decomposition. As can be observed in Figure7c, the weight loss of about 5 % from 90 to 130 °C in the first step is attributed to the extrusion of physically absorbed water. The grafted UiO-66(Zr)-NH_2 (**V'**) and (3-glycidyloxypropyl)trimethoxysilane fragments on the surface of Fe_3O_4@TiO_2 yolk-shell (**IV**) are decomposed during the second and third steps weight loss (11.4/ 13.2 %, from 150 to 330 / 340 to 530 °C), respectively. Thus, the amount of organic segments is estimated to be 0.55 and 0.65 mmol/g.

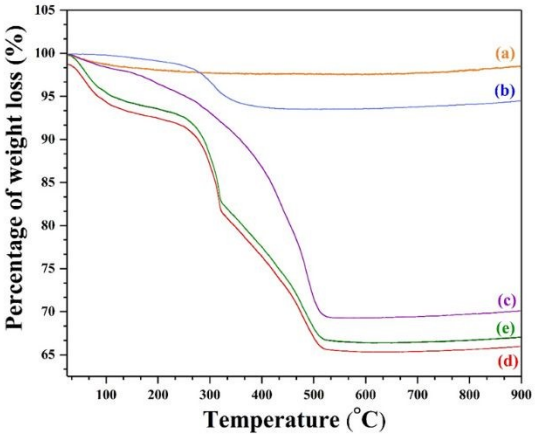

Fig. 7 TGA thermograms of (a) Fe_3O_4@TiO_2 yolk-shell (**IV**), (b) Fe_3O_4@TiO_2 YS-GLYMO (**V**), (c) Fe_3O_4@TiO_2 YS-GLYMO-UN (**VI**), (d) Fe_3O_4@TiO_2 YS-GLYMO-UNNi^{II} (**VII**) and the 7th recovered Fe_3O_4@TiO_2 YS-GLYMO-UNNi^{II} (**VII**) from the C-P cross-coupling reaction.

Room temperature magnetization curve of (a) Fe_3O_4@TiO_2 yolk-shell (**IV**) (b) fresh Fe_3O_4@TiO_2 YS-GLYMO-UNNi^{II} (**VII**) and the 7th recovered Fe_3O_4@TiO_2 YS-GLYMO-UNNi^{II} (**VI**) from the C-P bond construction are shown in (Figure 8 (a, b and c)), respectively. As demonstrated in (Figure 8), the value of saturation magnetic moments of Fe_3O_4@TiO_2 YS-GLYMO-UNNi^{II} (**VII**) is *Ms*= 15.33 emu g^{-1} which is lower than the value of Fe_3O_4@TiO_2 yolk-shell (**IV**) particles *Ms*= 43.06 emu g^{-1}. Saturation magnetization of Fe_3O_4@TiO_2 YS-GLYMO-UNNi^{II} (**VII**) was decreased as non-magnetic materials were present on the surface of Fe_3O_4@TiO_2 yolk-shell (**IV**).

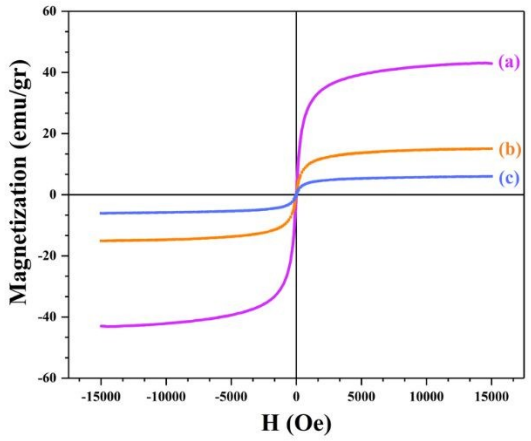

Fig. 8 Magnetization curves of (a) Fe_3O_4@TiO_2 yolk-shell (**IV**), (b) Fe_3O_4@TiO_2 YS-GLYMO-UNNi^{II} (**VII**) and (c) the 7th recovered Fe_3O_4@TiO_2 YS-GLYMO-UNNi^{II} (**VI**) from the C-P cross-coupling reaction.

3.2. Catalytic performance of the Fe_3O_4@TiO_2 YS-GLYMO-UNNi^{II} (VII) in the C-P cross-coupling reaction

In order to highlight the advantages of using this new nanostructured catalyst in organic synthesis, we applied it as the catalyst for C-P cross-coupling reaction after full characterization of the Fe_3O_4@TiO_2 YS-GLYMO-UNNi^{II} (**VII**) (Scheme 2). The reaction conditions were optimized systematically in our initial screening experiments. The results are presented in Table 1. The standard reaction of C-P cross-coupling was performed using iodobenzene with diethylphosphite as the initial study. The optimized reaction conditions were obtained by investigating the effect of different amounts of catalyst loadings, various molar ratios of iodobenzene/ diethylphosphite, several bases and different temperatures. In the absence of either the base (in solvent-free conditions at 100 °C, Table 1, entry 1) or the catalyst (in the presence of WERSA (2.5 mL) at 100 °C, Table 1, entry 2), no reasonable yield of the C-P cross-coupling product was

obtained even after a long period of time. The influence of the catalyst loading on the reaction rate and yield was investigated by applying 1 /1.9, 2 and 2.1 molar ratio of iodobenzene/ diethylphosphite under the temperature range of 80-100 °C in the presence of water extract of rice straw ash (WERSA) (2.5 mL) (Table 1, entries 3-11).Furthermore, the reaction of iodobenzene with diethylphosphite in the presence of 0.4 mol% of nanocatalyst at 90 °C and ground water (Damavand Mineral Water was used as a source of ground water) was done (Table 1, entry 12). As can be clearly observed, the reaction was better performed in the presence of WERSA rather than ground water.

It is evident that the best result in the C-P cross-coupling reaction were achieved by carrying out the reaction by applying 1/1.2 molar ratio of iodobenzene/ diethylphosphite, WERSA (2.5 mL) and 0.4 mol% of nanocatalyst at 90 °C (Table 1, entry 9). In addition, some different bases such as Et_3N, K_2CO_3, *i*-Pr_2NH, NaOAc, morpholine, and NaOH were studied and it was found that they did not improve the yield or reaction rate significantly (Table 1, entries 13-18). Next, in the C-P cross-coupling reaction, the unique catalytic behaviour of Fe_3O_4@TiO_2 YS-GLYMO-UNNi^{II} (**VII**) was shown by examining the model reaction in the presence of Fe_3O_4 NPs (**I**), Fe_3O_4@SiO_2 (**II**), Fe_3O_4@SiO_2@TiO_2 (**III**), Fe_3O_4@TiO_2 YS (**IV**), Fe_3O_4@TiO_2 YS-GLYMO (**V**), Fe_3O_4@TiO_2 YS-GLYMO-UN (**VI**), $Ni(OAc)_2$ and UiO-66(Zr)-NH_2 (**V'**) (Table 1, entries 19-26). Although reaction times were prolonged, no considerable yield was produced in the model reaction.

With suitable reaction conditions established (Table 1, entry 9), we next proceeded to assess the scope of C-P cross-coupling reaction of various activated and inactivated aryl halides/ aryl boronic acids including those containing electron-donating or electron-withdrawing groups, styrene and phenylacetylene with diethylphosphite/ triethylphosphite in the presence of Fe_3O_4@TiO_2 YS-GLYMO-UNNi^{II} (**VII**), the results of which are summarized in Table 2.

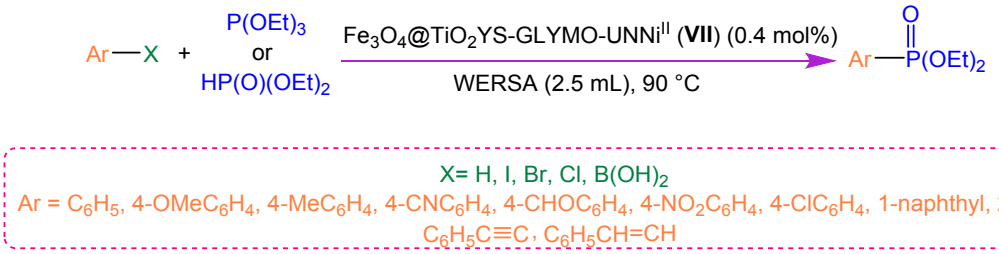

Scheme 2 Synthesis of arylphosphonates/ vinylphosphonate/ alkynylphosphonate via $C_{sp2/sp}$-P cross coupling reaction catalyzed by Fe_3O_4@TiO_2 YS-GLYMO-UNNi^{II} (**VII**).

Table 1 Optimization of reaction conditions for the C-P cross-coupling reaction of iodobenzene with diethylphosphite in the presence of Fe_3O_4@TiO_2 YS-GLYMO-UNNi^{II} (**VII**).

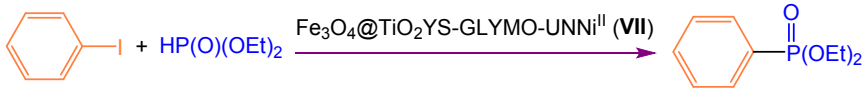

Entry	Amount of catalyst (mol%)	Molar ratios of Iodobenzene: Diethylphosphite	Base	Temperature (°C)	Time (h)	Isolated Yield (%)
1	-	1:2	-	100	24	-
2	-	1:2	WERSA (2.5 mL)	100	24	-
3	0.3	1:2	WERSA (2.5 mL)	100	2.5/24	80/80
4	0.3	1:1.9	WERSA (2.5 mL)	100	2.5/24	75/75
5	0.3	1:2.1	WERSA (2.5 mL)	100	2.25	95
6	0.4	1:2.1	WERSA (2.5 mL)	100	2.10	95
7	0.4	1:2.1	WERSA (2 mL)	100	2.30	80
8	0.4	1:2.1	WERSA (3 mL)	100	2.10	95
9	**0.4**	**1:2.1**	**WERSA (2.5 mL)**	**90**	2.10	**95**
10	0.5	1:2.1	WERSA (2.5 mL)	90	2.10	95
11	0.4	1:2.1	WERSA (2.5 mL)	80	2.30	85

View Article Online
DOI: 10.1039/C9NJ00352E

12	0.4	1:2.1	Ground water (2.5 mL)	90	24	75
13[a]	0.4	1:2.1	Et_3N	90	24	85
14[a]	0.4	1:2.1	K_2CO_3	90	24	45
15[a]	0.4	1:2.1	*i*-Pr_2NH	90	24	65
16[a]	0.4	1:2.1	NaOAc	90	24	50
17[a]	0.4	1:2.1	Morpholine	90	24	40
18[a]	0.4	1:2.1	NaOH	90	24	35
19[b]	0.3 g	1:2.1	WERSA (2.5 mL)	90	24	-
20[c]	0.3 g	1:2.1	WERSA (2.5 mL)	90	24	-
21[d]	0.3 g	1:2.1	WERSA (2.5 mL)	90	24	trace
22[e]	0.3 g	1:2.1	WERSA (2.5 mL)	90	24	20
23[f]	0.3 g	1:2.1	WERSA (2.5 mL)	90	24	25
24[g]	0.3 g	1:2.1	WERSA (2.5 mL)	90	24	35
25[h]	0.3 g	1:2.1	WERSA (2.5 mL)	90	24	40
26[i]	0.3 g	1:2.1	WERSA (2.5 mL)	90	24	trace

The reaction was performed in the presence of [a] base (1.5 mmol), [b] Fe_3O_4 NPs (**I**), [c] $Fe_3O_4@SiO_2$ (**II**), [d] $Fe_3O_4@SiO_2@TiO_2$ (**III**), [e] $Fe_3O_4@TiO_2$ YS (**IV**), [f] $Fe_3O_4@TiO_2$ YS-GLYMO (**V**), [g] $Fe_3O_4@TiO_2$ YS-GLYMO-UN (**VI**), [h] $Ni(OAc)_2$ and [i] UiO-66(Zr)-NH_2 (**V'**).

The results in Table 2 revealed that the catalytic reaction of aryl iodides with diethylphosphite/ triethylphosphite (isolated yields 85-95%, entries1,4-9) proved to be more productive than aryl chloride and aryl bromides coupling reaction with diethylphosphite/ triethylphosphite (entries 2, 3, 10, 11). This might be due to the fact that in all of the cases, the reactions with aryl iodides are faster than that of aryl bromide or aryl chloride as the result of lower C-I bond strength *vs.* C-Br and C-Cl bonds. Furthermore, aryl iodides reactions containing electron-withdrawing groups such as -NO_2, -Cl, -CN and -CHO were completed faster with excellent yields in comparison with those containing electron-donating substituents such as -Me and -OMe (Table 2, entries 4-9). This method was also applicable for the reaction of some other aryl boronic acids, styrene, and phenylacetylene with diethylphosphite/ triethylphosphite (entries 12-16). It could be seen that aryl boronic acids with electron-withdrawing group (-Cl) participated in the C-P cross coupling reaction more quickly than the aryl boronic acids with electron-donating group (-CH_3) (Table 2, entries 13 and 14). As shown in Table 2, styrene reacted more quickly with diethylphosphite/ triethylphosphite than phenylacetylene and afforded the desired products in shorter reaction times (Table 2, entry 15 *vs* entry 16). As it can be seen throughout the whole table, aryl halides, aryl boronic acids, styrene, and phenylacetylene react faster with triethylphosphite than diethylphosphite.

Table 2 C-P cross-coupling reaction of aryl halides/ aryl boronic acids/ styrene/ phenylacetylene with diethylphosphite/ triethylphosphite in the presence of $Fe_3O_4@TiO_2$ YS-GLYMO-UNNi^{II} (**VII**) in green media.

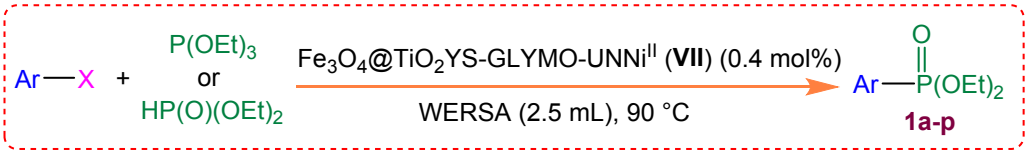

Entry	R	X	Time (h) of $HP(O)(OEt)_2$/ $P(OEt)_3$	Isolated Yield (%)
1	C_6H_5	I	2.10/1.15	95

View Article Online
DOI: 10.1039/C9NJ00352E

2	C_6H_5	Br	3/2	90
3	C_6H_5	Cl	5/3	85
4	4-$OMeC_6H_4$	I	4.30/2.40	90
5	4-MeC_6H_4	I	4/3	90
6	4-CNC_6H_4	I	3.20/2.20	85
7	4-$CHOC_6H_4$	I	3.40/3.10	85
8	4-$NO_2C_6H_4$	I	3/1.50	90
9	4-ClC_6H_4	I	3.30/3	85
10	1-naphthyl	Br	6/4.30	70
11	2-thienyl	Br	5/4	75
12	C_6H_5	$B(OH)_2$	4/3.20	85
13	4-ClC_6H_4	$B(OH)_2$	4.30/3.50	85
14	4-MeC_6H_4	$B(OH)_2$	6/5	85
15[a]	$C_6H_5CH=CH$	H	5.5/4.25	80
16[a]	$C_6H_5C\equiv C$	H	7.20/5.10	80

[a] Reaction condition: Fe_3O_4@TiO_2 YS-GLYMO-UNNi^{II} (**VII**) (0.6 mol %).

All of the synthesized compounds were known and isolated as oil products. Molecular ion peaks of all the prepared products showed their respective m/z based on mass spectrometric data. Furthermore, the structure of the selected compounds was further investigated by surveying their high-field ^{1}H NMR and ^{13} C NMR spectral data. The completion of the reaction, monitored by TLC, was confirmed when starting material began disappearing. (*See supporting information file for details*)

Scheme 3 shows the suggested mechanism for the C-P cross-coupling reaction. In the first step, the mechanism proceeded through oxidative addition of aryl halide to Fe_3O_4@TiO_2 YS-GLYMO-UNNi^{II} (**VII**) NPs which yielded intermediate **I** through the oxidation of Ni^{II} to Ni^{IV}. Upon the coordination of diethylphosphite/ triethylphosphite to intermediate **I**, the intermediate **II** produced after the deprotonation under basic condition or an Arbuzov type reaction that RX is eliminated from adduct **I'**. Finally, using the reductive elimination of intermediate **II** with the simultaneous release of Fe_3O_4@TiO_2 YS-GLYMO-UNNi^{II} (**VII**) for the next catalytic cycle, the intended coupling product (**III**) of C-P cross-coupling reaction was obtained.[106]

3.3. Heterogeneity studies

Hot filtration test

To investigate whether the reaction takes place at the surface of solid Ni species as a truly heterogeneous reaction or any Ni-leached species act as homogeneous catalyst, the hot filtration test was conducted under the optimal conditions. In this line, after half of the specified time for the C-P cross-coupling reaction passed, an external magnetic field was used to remove the nanostructured catalyst and then no nanostructured catalyst was used for the latter part of the reaction. Thin layer chromatography was performed to track the progress of the reaction. There was no further coupling reaction even after an extended time. As can be seen, an isolated yield of 63 % was achieved for the C-P cross-coupling reaction. The reaction mixture was analyzed using ICP-AES and the results showed that during C-P cross-coupling reactions, only 0.02 ppm of Ni species was leached out from the surface of Fe_3O_4@TiO_2 YS-GLYMO-UNNi^{II} (**VII**) NPs which in turn indicates that the nanostructured catalyst is heterogeneous. The results of hot filtration test for the C-P cross-coupling reaction were also presented in (Figure 9), indicating a strong attachment of Ni^{II} to the Fe_3O_4@TiO_2 YS-GLYMO-UN (**VI**) NPs surface.

Poisoning test

A poisoning test was carried out under the optimized reaction conditions in order to determine the homogeneity/heterogeneity of the catalyst. Ethylenediamine tetraacetic acid (EDTA), due to its high affinity to capture Ni^{II} ions causing the formation of a stable complex (**VI**), was used as an excellent scavenger (Scheme 4).[107] In this point, the model reaction was performed in two separate flasks while Fe_3O_4@TiO_2 YS-GLYMO-UNNi^{II} (**VII**) was present in both of them and EDTA (250 mg) was present in one flask and absent in another. The progress of the reaction was monitored by TLC. Time-dependent correlation showed that the improvement of the product yield of the reaction did not experience any significant

changes while ethylenediamine tetraacetic acid (EDTA) was present (Figure 10).

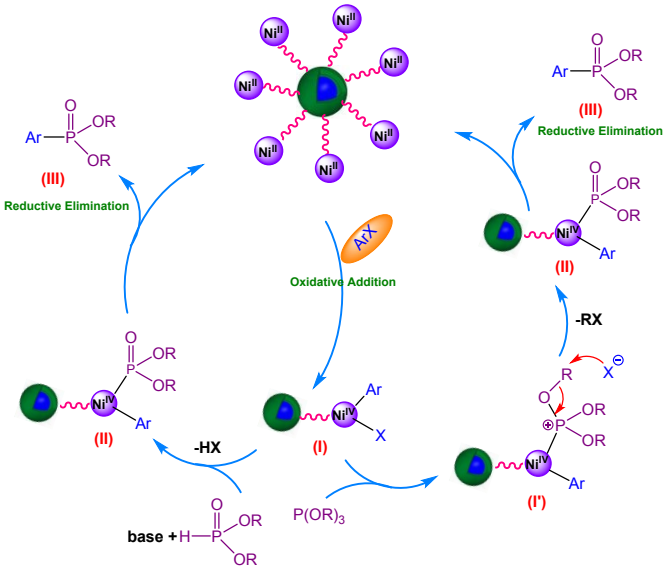

Scheme 3 Plausible mechanism for the C-P cross coupling reaction in the presence of Fe_3O_4@TiO_2 YS-GLYMO-UNNi^{II} (**VII**).

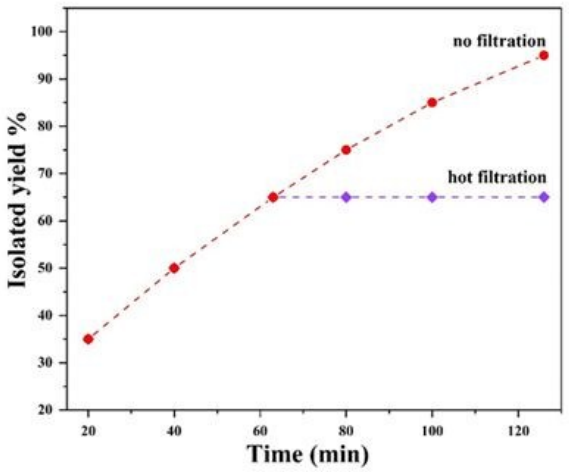

Fig. 9 Hot filtration experiment in the model reaction of the C-P cross-coupling reaction using Fe_3O_4@TiO_2 YS-GLYMO-UNNi^{II} (**VII**).

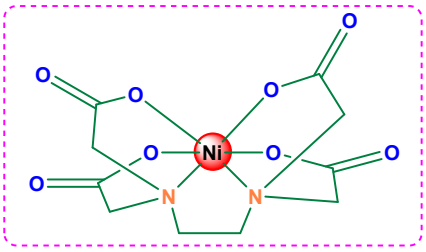

Scheme 4 The chemical structure of the Nickel(II) EDTA complex (**VI**).

This means that Ni^{II} did not leach during the course of the reaction into the reaction media which in turn proved that the catalyst is truly heterogeneous. In view of industrial purposes and green chemistry, reusability is one of the most important properties of metal catalysis that should be considered. Incidentally, the reusability of Fe_3O_4@TiO_2 YS-GLYMO-UNNi^{II} (**VII**) was studied by consecutive C-P cross-coupling reaction of iodobenzene with diethylphosphite under the optimized reaction conditions. After the first catalytic run, the nanostructured catalyst was separated by an external magnetic field from the reaction mixture, washed with EtOAc (3 × 10 mL) and dried at 70 °C for 24 h. Next, a new C-P cross-coupling reaction of fresh reactants was started by the recovered nanostructured catalyst. As can be clearly observed in Figure 11, the nanostructured catalyst was reusable for up to seven cycles through the catalytic reaction and an insignificant decrease in the yields was detected in the 6th and 7th runs.

Several techniques were used to confirm the great stability and reusability of this nanostructured catalyst including Fourier transform infrared (FT-IR) spectroscopy, X-ray diffraction (XRD) analysis, thermogravimetric analysis (TGA), vibrating sample magnetometry (VSM) and inductively coupled plasma atomic emission spectroscopy (ICP-AES).

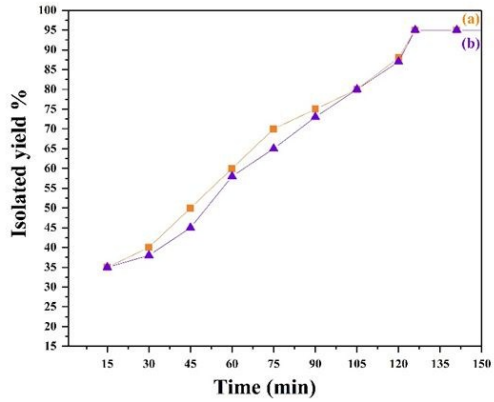

Fig. 10 Product yield as a function of reaction time catalyzed by Fe_3O_4@TiO_2 YS-GLYMO-UNNi^{II} (**VII**) in (a) the presence and (b) the absence of EDTA.

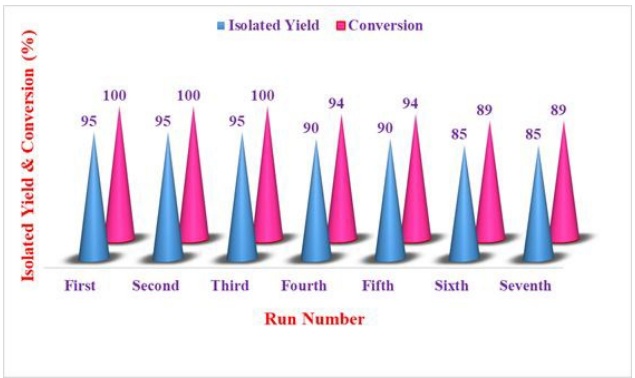

Fig. 11 C-P cross-coupling reaction of iodobenzene with diethylphosphite under the optimized reaction condition catalyzed by the 7th recycled Fe_3O_4@TiO_2 YS-GLYMO-UNNi^{II} (**VII**).

There were no signs of any significant changes in the intensities, frequencies and shapes of absorption bands in the FT-IR spectra of the 7th recovered Fe_3O_4@TiO_2 YS-GLYMO-UNNi^{II} (**VII**) from the C-P cross-coupling reaction, but it could be clearly pointed out that nickel ions were in a strongly coordination with organic moieties on the surface of to the Fe_3O_4@TiO_2 YS-GLYMO-UN (**VI**) NPs (Figure 1h). During the C-P cross-coupling reaction process, the nanostructured catalyst was also revealed to undergo no changes when XRD was used to analyse the 7th recovered catalyst. Based on Debye-Scherrer equation, the average crystalline size of the 7th recovered Fe_3O_4@TiO_2 YS-GLYMO-UNNi^{II} (**VII**) was 32 nm (Figure 2d). After seven runs from the C-P cross-coupling reaction, the stability of Fe_3O_4@TiO_2 YS-GLYMO-UNNi^{II} (**VII**) was analysed using thermogravimetric analysis. It could be concluded that insignificant differences were detected in the decomposition pattern (compare Figure7d with 7e). However, the weight loss of the grafted organic motif in second and third steps were decreased from 11.4/13.2 % (in the fresh nanocatalyst) to 10.4/12.2 % in the 7th recovered nanocatalyst. Accordingly, the amount of the grafted UiO-66(Zr)-NH_2 (**V'**) and (3-glycidyloxypropyl)trimethoxysilane were decreased from 0.55/0.65 to 0.52/0.60 mmol/g after seven runs, which might be attributed to the diminutive leaching of organic fragments during recycling process.

As shown in Figure 8c, the saturation magnetization values (*Ms*) of the 7th recovered Fe_3O_4@TiO_2 YS-GLYMO-UNNi^{II} (**VII**) from C-P cross-coupling reaction is *Ms*= 7.88 emu g^{-1} which is relatively lower than the fresh nanostructured catalyst value (*Ms*= 15.33 emu g^{-1}). It is noteworthy to mention that after seven runs from the C-P cross-coupling reaction, the superparamagnetic behaviour of the recovered Fe_3O_4@TiO_2 YS-GLYMO-UNNi^{II} (**VII**) still holds true.

In order to quantitatively analyse and determine the exact amount of nickel in the fresh and the 7th reused Fe_3O_4@TiO_2 YS-GLYMO-UNNi^{II} (**VII**), ICP-AES technique has been used. The freshly-prepared nanostructured catalyst was shown to contain 0.86 mmol of nickel per 1.000 g of Fe_3O_4@TiO_2 YS-GLYMO-UNNi^{II} (**VII**), whereas the 7th recovered nanostructured catalyst from C-P cross-coupling reaction contained 0.80 mmol of Ni per 1.000 g of the nanostructured catalyst after ICP-AES analysis. After seven runs, the results indicate that 93 % of Ni^{II} could be found in the structure of the catalyst. The data also revealed that an insignificant amount of nickel leached from the surface of Fe_3O_4@TiO_2 YS-GLYMO-UNNi^{II} (**VII**). Based on the above analysis, the strong chelating action of active sites on the surface of Fe_3O_4@TiO_2 YS-GLYMO-UN (**VI**) NPs probably caused the high catalytic activity and excellent reusability of Fe_3O_4@TiO_2 YS-GLYMO-UNNi^{II} (**VII**).

Finally, to prove how the advantages of the present method for the synthesis of arylphosphonates, vinylphosphonate and alkynylphosphonate outweighs that of those reported in the literature for the synthesis of these important scaffolds (Table 3), we compared the results of C-P cross-coupling reaction in the presence of various catalytic systems. Several factors were studied including catalyst loading, solvent, temperature, reaction time, different kinds of phosphite ester, and the yield of the product. As opposed to other catalytic systems, Fe_3O_4@TiO_2 YS-GLYMO-UNNi^{II} (**VII**) is a palladium-free and magnetic nanostructured catalyst, the separation of which is easily done using a magnetic field. Additionally, another merit of this nanostructured catalyst is that it is capable of working in water extract of rice straw ash (WERSA) without needing such additives as SDS (sodium dodecyl sulphate),[23] TBAB (tetrabutylammonium bromide),[35] Zn,[32] iso-propanol[27] or activation by microwave irradiation.[33, 34, 40, 54, 55, 106]

Table 3 Comparison of the catalytic activity of Fe_3O_4@TiO_2 YS-GLYMO-UNNi^{II} (**VII**) with some literature precedents for C-P cross-coupling reaction.

Entry	Phosphite ester	X	Catalyst	Catalyst loading (mol%)	Conditions	Time (h)	Yield (%)	Ref.
1	$HP(O)(OEt)_2$	$B(OH)_2$	Cu_2O/1,10-phenanthroline	10	(*i*-Pr)$_2$NEt, CH_3CN, r.t, air	24	47-96	13
2	$HP(O)(OEt)_2$ $HP(O)(OMe)_2$ $HP(O)(OBu)_2$	B(pin)	$Pd(OAc)_2$	5	TMACl[a], Ag_2CO_3, EtOH, 80 °C, N_2	24	18-89	14
3	$HP(O)(OEt)_2$ $HP(O)(OMe)_2$ $HP(O)(i\text{-}OPr)_2$	$B(OH)_2$	Copper (II) complex	10	KOAc, THF, r.t	72	56-83	15
4	$HP(O)(OEt)_2$ $HP(O)(OBu)_2$ $HP(O)(OBn)_2$	Br	$Pd(OAc)_2$	5-10	NEt_3, EtOH, MW (110-120-150 °C)	15-30 min	68-87	106

View Article Online
DOI: 10.1039/C9NJ00352E

	$HP(O)(Ph)_2$							
5	$HP(O)(OEt)_2$ $HP(O)(i\text{-}OPr)_2$ $HP(O)(n\text{-}Bu)_2$	Br	$Pd(OAc)_2$, $PdCl_2$, $Pd(PPh_3)_4$	2	NEt_3 or pyridine or n-Bu_3N, 90 or 100 °C, toluene	12 min-64 h	3-98	108
6	$HP(O)(OEt)_2$	Br	$Pd(OAc)_2/PPh_3$	2, 5, 10, 13, 15	NEt_3	24-60	37-93	25
7	$P(OEt)_3$	I, Br	$PdCl_2$, $NiCl_2$	10	MW (80-120 °C)	5 min	60-98	54
8	$P(OEt)_3$ $P(i\text{-}OPr)_3$	I, Br, Cl	$PdCl_2$	4.4	TBAB, n-Pr_3N, H_2O, 100 °C	1-12	65-99	35
9	$HP(O)(OEt)_2$	I	$Pd(OAc)_2$/ dpephos[b]	5	$Ag[P(O)(OEt)_2]$, THF, 25 °C	16	44-92	39
10	$HP(O)(OEt)_2$ $P(O)(OBu)_2$ $HP(O)Ph_2$	Br	$Pd(OAc)_2$	(5, 10)	solvent-free, Et_3N, MW (150-200 °C)	4.8-15 min	41-95	40
11	$P(OEt)_3$	I, Br, Cl, OTs, $B(OH)_2$	Pd-imino-Py-γ-Fe_2O_3	0.1	H_2O, Et_3N, 100 °C	1-15	57-98	37
12	$P(OEt)_3$, $HP(O)(OEt)_2$ HP(O)(OPh)2	I, Br, Cl, OTs, $B(OH)_2$	Pd-BIP-γ-Fe_2O_3@SiO_2	2	Et_3N, 100 °C, solvent-free	4-15	46-91	23
13	$P(OEt)_3$, $HP(O)(OEt)_2$, $P(OPh)_3$, $HP(O)(Ph)_2$, $P(i\text{-}OPr)_3$, $HP(O)(i\text{-}OPr)_2$	I, Br, Cl OTs, $B(OH)_2$	Pd-DABCO-γ-Fe_2O_3	0.07 - 0.1	H_2O, Et_3N, 100 °C	1-15	51-98	24
14	$P(OPh)_3$ $HP(O)(OEt)_2$ $HP(O)(OPh)_2$ $HP(O)(i\text{-}OPr)_2$	I, Br, Cl, OTs, $B(OH)_2$	Pd-2-ATP-γ-Fe_2O_3	0.1	H_2O, SDS, 100 °C	1.5-8	51-97	23

View Article Online DOI: 10.1039/C9NJ00352E

15	$HP(O)(Ph)_2$	I, Br	$NiCl_2.6H_2O$	10, 20	H_2O, Zn, 2,2'- bipyridine, 70 °C	15-24	75-97	32
16	$HP(O)Ph_2$	I, Br, Cl	Pd/C	1	H_2O, K_2CO_3, MW (180 °C)	1	18-87	33
17	$HP(O)(i\text{-}OPr)_2$ $HP(O)(Ph)_2$	I, Br, Cl	Palladacycle[c] (II), (1)/ Palladacycle (I)/X-Phos[d]	1	H_2O, TBAB, KF, reflux, *i*-PrOH, N_2	16	53-99, 35-99/65-99	27
18	$HP(O)(OEt)_2$	I, Br, OTf	$Pd(OAc)_2$/dppf[e]	10	THF, Et_3N, KOAc, 68 °C	1.5-32	63-98	22
19	$HP(O)(OEt)_2$ $HP(O)(OMe)_2$ $HP(O)(O\text{-}iPr)_2$	Br	$Pd(PPh_3)_4$	5	THF, Cs_2CO_3 or Et_3N, MW (120 °C)	10 min	72-96	33
20	$HP(O)(OEt)_2$ $HP(O)Ph_2$	I, Br	$Pd(OAc)_2$	5, 10	Solvent free, Et_3N, MW (150-200 °C)	1.8-15 min	27-93	34
21	$HP(O)(iPr)_2$	I, Br, OTf	$Pd(OAc)_2$/dppf	1	DMF, 110 ºC or MeCN, reflux, $(iPr)_2NEt$	24	27-92	27
22	$HPO(OEt)_2$	Br	$Pd(OAc)_2/PPh_3$	2	EtOH, $(cyclohexyl)_2MeN$, reflux	16	80-93	38
23	$HP(O)(OEt)_2$	$B(OH)_2$	$Pd(OAc)_2$/dmphen[f]	2	DMF, P-BQ, MW (100 °C)	30 min	51-90	55
24	$P(OEt)_3$, $HP(O)(OEt)_2$	I, Br, Cl, H, $B(OH)_2$	Fe_3O_4@TiO_2 YS-GLYMO-UNNi^{II} (**VII**)	0.4, 0.6	WERSA, 90 °C	1.15-7.20	70-95	Present study

[a] Tetramethylammonium chloride. [b] Dpephos = (Oxydi-2,1-phenylene)bis(diphenylphosphine). [c] Cyclopalladated ferrocenylimine. [d] 2-(Dicyclohexylphosphanyl)-2 ,4,6-tri-*iso*-propyl-1,1-biphenyl. [e] 1,1'-bis(diphenylphosphino)ferrocene. [f] 2,9-dimethyl-1,10-phenanthroline.

4. Conclusion

In summary, the synthesis of Ni^{II} immobilized on aminated Fe_3O_4@TiO_2 yolk-shell NPs functionalized by (3-glycidyloxypropyl)trimethoxysilane (Fe_3O_4@TiO_2 YS-GLYMO-UNNi^{II} (**VII**)) was successfully done from readily available starting materials. Spectroscopic and microscopic techniques were used to characterize Fe_3O_4@TiO_2 YS-GLYMO-UNNi^{II} (**VII**) and the results revealed that the new nanostructured catalyst is spherical in shape, has an average particle size of 30-32 nm, and shows superparamagnetic behaviour. In the next step, it was applied as a magnetically recyclable heterogeneous nanostructured catalyst for the C-P cross coupling reaction in the presence of water extract of rice straw ash (WERSA). The merits of the suggested methodology include but not limited to the following features: eco-friendliness, simplicity, excellent yields of products, short reaction times, mild reaction conditions, high efficiency, easy separation of the catalyst with the assistance of an external magnetic field and reusability of the nanostructured catalyst for up to seven cycles without significant degradation in activity. All these features make this approach quite efficient for the preparation of arylphosphonates/ vinylphosphonate/ alkynylphosphonate acridinedione derivatives as an important class of organophosphorus compounds.

Conflicts of interest

There are no conflicts to declare.

Acknowledgements

The authors gratefully acknowledge the partial support of this study by Ferdowsi University of Mashhad Research Council (Grant no. p/3/43366).

Notes and references

1 L. D. Quin, A Guide to Organophosphorus Chemistry; Wiley Interscience, New York, 2000.
2 P. J. Murphy, Ed. Organophosphorus Reagents; Oxford University Press: Oxford, U.K., 2004.
3 W. Tang and X. Zhang, *Chem. Rev.*, 2003, **103**, 3029-3070.

4 Y. C. Kim, S. G. Brown, T. K. Harden, J. L. Boyer, G. Dubyak, B. F. King, G. Burnstock and K. Jacobson, *J. Med. Chem.*, 2001, **44**, 340-349.
5 J. J. Shie, J. M. Fang, S. Y. Wang, K. C. Tsai, Y. S. Cheng, A. S. Yang, S. C. Hsiao, C. Y. Su and C. H. Wong, *J. Am. Chem. Soc.*, 2007, **129**, 11892-11893.
6 T. S. Kumar, S. Y. Zhou, B. V. Joshi, R. Balasubramanian, T. H. Yang, B. T. Liang and K. A. Jacobson, *J. Med. Chem.*, 2010, **53**, 2562-2576.
7 H. H. Chou and C. H. Cheng, *Adv. Mater.*, 2010, **22**, 2468-2471.
8 F. M. Hsu, C. H. Chien, C. F. Shu, C. H. Lai, C. C. Hsieh, K. W. Wang and P. T. Chou, *Adv. Funct. Mater.*, 2009, **19**, 2834-2843.
9 T. Baumgartner and R. Reau, *Chem. Rev.*, 2006, **106**, 4681-4727.
10 R. Engel, *Chem. Rev.*, 1977, **77**, 349-367.
11 H. A. McManus and P. J. Guiry, *Chem. Rev.*, 2004, **104**, 4151-4202.
12 P. W. N. M. van Leeuwen, P. C. J. Kamer, J. N. H. Reek and R. Dierkes, *Chem. Rev.*, 2000, **100**, 2741-2770.
13 R. Zhuang, J. Xu, Z. Cai, G. Tang, M. Fang and Y. Zhao, *Org. Lett.*, 2011, **13**, 2110-2113.
14 T. H. Chen, D. M. Reddy and C. F. Lee, *RSC Adv.*, 2017, **7**, 30214-30220.
15 H. Wan, Y. Zhao, Q. Wang, Y. Zhang and Y. Li, *Russ. J. Gen. Chem.*, 2016, **86**, 150-153.
16 P. Liua, J. Yanga, P. Lia and L. Wanga, *Appl. Organometal. Chem.*, 2011, **25**, 830‑835.
17 Q. Gui, L. Hu, X. Chen, J. Liu and Z. Tan, *Chem. Commun.*, 2015, **51**, 13922-13924.
18 D. Julienne, J. F. Lohier, O. Delacroix and A. C. Gaumont, *J. Org. Chem.*, 2007, **72**, 2247-2250.
19 T. Yuan, F. Chen and G. P. Lu, *New J. Chem.*, 2018, **42**, 13957-13962.
20 J. Gu and C. Cai, *Org. Biomol. Chem.*, 2017, **15**, 4226-4230.
21 D. Julienne, O. Delacroix and A. C. Gaumont, *Phosphorus, Sulfur Silicon Relat. Elem.*, 2009, **184**, 846-856.
22 M. Kalek, M. Jezowska and J. Stawinski, *Adv. Synth. Catal.*, 2009, **351**, 3207-3216.
23 S. Sobhani and Z. Zeraatkar, *Appl. Organometal. Chem.*, 2016, **30**, 12‑19.
24 S. Sobhani and Z. Vahidi, *Can. J. Chem.*, 2017, **95**, 1280-1284.
25 A. Bessmertnykh, C. M. Douaihy and R. Guilard, *Chem. Lett.*, 2009, **38**, 738-739.
26 K. Xu, F. Yang, G. Zhang and Y. Wu, *Green Chem.*, 2013, **15**, 1055-1060.
27 Y. Belabassi, S. Alzghari and J. L. Montchamp, *J. Organomet. Chem.*, 2008, **693**, 3171-3178.
28 J. Li, M. Lutz, A. L. Spek, G. P.M. van Klink, G. van Koten and R. J. M. K. Gebbink, *J. Organomet. Chem.*, 2010, **695**, 2618-2628.
29 C. Shen, G. Yang and W. Zhang, *Org. Biomol. Chem.*, 2012, **10**, 3500-3505.
30 A. Stadler and C. O. Kappe, *Org. Lett.*, 2002, **4**, 3541-3543.
31 M. Kalek, A. Ziadi and J. Stawinski, *Org. Lett.*, 2008, **10**, 4637-4640.
32 X. Zhang, H. Liu, X. Hu, G. Tang, J. Zhu and Y. Zhao, *Org. Lett.*, 2011, **13**, 4850-4853.
33 S. M. Rummelt, M. Ranocchiari and J. A. van Bokhoven, *Org. Lett.*, 2012, **14**, 2188-2190.
34 G. Keglevich, E. Jablonkai and L. B. Balázs, *RSC Adv.*, 2014, **4**, 22808-22816.
35 N. Iranpoor, H. Firouzabadi, K. R. Moghadam and S. Motavalli, *RSC Adv.*, 2014, **4**, 55732-55737.
36 S. Sobhani, Z. Vahidi, Z. Zeraatkar and S. Khodadadi, *RSC Adv.*, 2015, **5**, 36552-36559.
37 S. Sobhani and Z. Ramezani, *RSC Adv.*, 2016, **6**, 29237-29244.
38 L. J. Gooßen and M. K. Dezfuli, *Synlett*, 2005, **2005**, 445-448.
39 M. C. Kohler, J. G. Sokol and R. A. Stockland, *Tetrahedron Lett.*, 2009, **50**, 457-459.
40 E. Jablonkai and G. Keglevich, *Tetrahedron Lett.*, 2013, **54**, 4185-4188.
41 H. Y. Zhang, M. Sun, Y. N. Ma, Q. P. Tian and S. D. Yang, *Org. Biomol. Chem.*, 2012, **10**, 9627-9633.
42 M. Stankevič and A. Włodarczyk, *Tetrahedron*, 2013, **69**, 73-81.
43 K. Xu, H. Hu, F. Yang and Y. Wu, *Eur. J. Org. Chem.*, 2013, **2013**, 319-325
44 A. J. Bloomfield and S. B. Herzon, *Org. lett.*, 2012, **14**, 4370-4373.
45 E. L. Deal, C. Petit and J. L. Montchamp, *Org. lett.*, 2011, **13**, 3270-3273.
46 D. S. Glueck, *Chem. Eur. J.*, 2008, **14**, 7108-7117.
47 K. D. Berlin and G. B. Butler, *Chem. Rev.*, 1960, **60**, 243-260.
48 A. L. Schwan, *Chem. Soc. Rev.*, 2004, **33**, 218-224.
49 I. P. Beletskaya and A. V. Cheprakov, *Coord. Chem. Rev.*, 2004, **248**, 2337-2364.
50 K. M. Pietrusiewicz and M. Zablocka, *Chem. Rev.*, 1994, **94**, 1375-1411.
51 D. S. Glueck, *Synlett*, 2007, **2007**, 2627-2634.
52 A. Grabulosa, J. Granell and G. Muller, *Coord. Chem. Rev.*, 2007, **251**, 25-90.
53 J. J. Feng, X. F. Chen, M. Shi and W. L. Duan, *J. Am. Chem. Soc.*, 2010, **132**, 5562-5563.
54 D. Villemin, A. Elbilali, F. Siméon, P. A. Jaffrès, G. Maheut, M. Mosaddak and A. Hakiki, *J. Chem. Research (S)*, 2003, **7**, 436-437.
55 M. Andaloussi, J. Lindh, J. Sävmarker, P. J. R. Sjöberg and M. Larhed, *Chem. Eur. J.*, 2009, **15**, 13069-13074.
56 V. Polshettiwar, R. Luque, A. Fihri, H. Zhu, M. Bouhrara and J. M. Basset, *Chem. Rev.*, 2011, **111**, 3036-3075.
57 L. Zhou, C. Gao and W. Xu, *Langmuir*, 2010, **26**, 11217-11225.
58 J. Kim, J. E. Lee, J. Lee, J. H. Yu, B. C. Kim, K. An, Y. Hwang, C. H. Shin, J. G. Park, J. Kim and T. Hyeon, *J. Am. Chem. Soc.*, 2006, **128**, 688-689.
59 B. Liu, W. Zhang, F. Yang, H. Feng and X. Yang, *J. Phys. Chem. C*, 2011, **115**, 15875-15884.
60 H. M. Tanuraghaj and M. Farahi, *RSC Adv.*, 2018, **8**, 27818-27824.
61 R. B. Nasir Baig and R. S. Varma, *ACS Sustain. Chem. Eng.*, 2014, **2**, 2155-2158.
62 R. B. Nasir Baig and R. S. Varma, *Ind. Eng. Chem. Res.*, 2014, **53**, 18625-18629.
63 C. M. Fan, L. F. Zhang, S. S. Wang, D. H. Wang, L. Q. Lu and A. W. Xu, *Nanoscale*, 2012, **4**, 6835-6840.
64 J. Liu, J. Cheng, R. Che, J. Xu, M. Liu and Z. Liu, *J. Phys. Chem. C*, 2013, **117**, 489-495.

65 S. Liu, M. Xie, Y. Li, X. Guo, W. Ji, W. Ding and C. Au, *Sens. Actuator B-Chem.*, 2010, **151**, 229-235.
66 C. C. Huang, W. Huang and C. S. Yeh, *Biomaterials*, 2011, **32**, 556-564.
67 R. Purbia and S. Paria, *Nanoscale*, 2015, **7**, 19789-19873.
68 H. Li, M. Eddaoudi, M. O'Keeffe and O. M. Yaghi, *Nature*, 1999, **402**, 276-279.
69 J. L. C. Rowsell and O. M. Yaghi, *Micropor. Mesopor. Mater.*, 2004, **73**, 3-14.
70 Z. Q. Li, L. G. Qiu, T. Xu, Y. Wu, W. Wang, Z. Y. Wu and X. Jiang, *Mater. Lett.*, 2009, **63**, 78-80.
71 S. Gao, N. Zhao, M. Shu and S. Che, *Appl. Catal. A: Gen.*, 2010, **388**, 196-201.
72 F. Song, C. Wang, J. M. Falkowski, L. Ma and W. Lin, *J. Am. Chem. Soc.*, 2010, **132**, 15390-15398.
73 J. Gascon, U. Aktay, M. D. Hernandez-Alonso, G. P. M. van Klink and F. Kapteijn, *J. Catal.*, 2009, **261**, 75-87.
74 P. Serra-Crespo, E. V. Ramos-Fernandez, J. Gascon and F. Kapteijn, *Chem. Mater.,* 2011, **23**, 2565-2572.
75 N. T. S. Phan, K. K. A. Le and T. D. Phan, *Appl. Catal. A: Gen.*, 2010, **382**, 246-253.
76 F. X. L. I. Xamena, A. Abad, A. Corma and H. Garcia, *J. Catal.*, 2007, **250**, 294-298.
77 P. Li, S. Regati, R. J. Butcher, H. D. Arman, Z. Chen, S. Xiang, B. Chen and C. G. Zhao., *Tetrahedron Lett.*, 2011, **52**, 6220-6222.
78 M. Savonnet, S. Aguado, U. Ravon, D. Bazer-Bachi, V. Lecocq, N. Bats, C. Pinel and D. Farrusseng, *Green Chem.*, 2009, **11**, 1729-1732.
79 N. Razavi and B. Akhlaghinia, *RSC Adv.*, 2015, **5**, 12372-12381.
80 S. S. E. Ghodsinia and B. Akhlaghinia, *RSC Adv.*, 2015, **5**, 49849-49860.
81 M. Zarghani and B. Akhlaghinia, *Appl. Organomet. Chem.*, 2015, **29**, 683-689.
82 R. Jahanshahi and B. Akhlaghinia, *RSC Adv.*, 2015, **5**, 104087-104094.
83 N. Y. Siavashi, B. Akhlaghinia and M. Zarghani, *Res. Chem. Intermed.*, 2016, **42**, 5789-5806.
84 R. Jahanshahi and B. Akhlaghinia, *RSC Adv.*, 2016, **6**, 29210-29219.
85 M. Zarghani and B. Akhlaghinia, *RSC Adv.*, 2016, **6**, 31850-31860.
86 M. Zarghani and B. Akhlaghinia, *RSC Adv.*, 2016, **6**, 38592-38601.
87 M. Zarghani and B. Akhlaghinia, *Bull. Chem. Soc. Jpn.*, 2016, **89**, 1192-1200.
88 Z. Zarei and B. Akhlaghinia, *RSC Adv.*, 2016, **6**, 106473-106484.
89 M. Zamani, B. Akhlaghinia and A. Mohammadinezhad, *ChemistrySelect*, 2018, **3**, 9431-9442.
90 A. Mohammadinezhad and B. Akhlaghinia, *Aust. J. Chem.*, 2018, **71**, 32-46.
91 A. Mohammadinezhad and B. Akhlaghinia, *Green Chem.*, 2017, **19**, 5625-5641.
92 Z. Zareie and B. Akhlaghinia, *New J. Chem.*, 2017, **41**, 15485-15500.
93 N. Mohammadian and B. Akhlaghinia, *Res. Chem. Intermed.*, 2018, **44**, 1085-1103.
94 Z. Zarei and B. Akhlaghinia, *Turk. J. Chem.*, 2018, **42**, 170-191.
95 M. S. Ghasemzadeh and B. Akhlaghinia, *Bull. Chem. Soc. Jpn.*, 2017, **90**, 1119-1128.
96 M. S. Ghasemzadeh and B. Akhlaghinia, *ChemistrySelect*, 2018, **3**, 3161-3170.
97 M. S. Ghasemzadeh and B. Akhlaghinia, *ChemistrySelect*, 2019, **4**, 1542-1555.
98 S. Pakdel, B. Akhlaghinia and A. Mohammadinezhad, *ChemistryAfrica*, 2019, doi.org/10.1007/s42250-019-00042-5.
99 H. Karimzadegan, B. Akhlaghinia and M. S. Ghasemzadeh, *IJC*, 2019, in press.
100 B. Akhlaghinia, P. Sanati, A. Mohammadinezhad and Z. Zarei, *Res. Chem. Intermed.*, 2019, doi. 10.1007/s11164-019-03788-2.
101 J. Liu, J. Xu, R. Che, H. Chen, M. Liu and Z. Liu, *Chem. Eur. J.*, 2013, **19**, 6746-6752.
102 L. Shen, S. Liang, W. Wu, R. Lianga and L. Wu, *Dalton Trans.*, 2013, **42**, 13649-13657.
103 P. R. Boruah, A. A. Ali, M. Chetia, B. Saikia and D. Sarma, *Chem. Commun.*, 2015, **51**, 11489-11492.
104 Y. Wang, L. Wang, W. Huang, T. Zhang, Xi. Hu, J. A. Perman and S. Ma, *J. Mater. Chem. A*, 2017, **5**, 8385-8393.
105 J. Zhang, T. Xi, D. Zhao, Y. Cui, Y. Yang and G. Qian, *Sens. Actuator B-Chem.*, 2018, **260**, 63-69.
106 G. Keglevich, R. Henyecz, Z. Mucsi and N. Z. Kiss, *Adv. Synth. Catal.*, 2017, **359**, 4322-4331.
107 J. K. Nyborg and O. B. Peersen, *Biochem. J.*, 2004, **381**, 3-4.
108 T. Hirao, T. Masunaga and N. Yamada, *Bull. Chem. Soc. Jpn.*, 1982, **55**, 909-913.

View Article Online
DOI: 10.1039/C9NJ00352E

C-P bond construction catalyzed by Ni^{II} immobilized on aminated $Fe_3O_4@TiO_2$ yolk-shell NPs functionalized by (3-glycidyloxypropyl)trimethoxysilane ($Fe_3O_4@TiO_2$YS-GLYMO-UNNi^{II}) in green media

Maryam Sadat Ghasemzadeh, [a] Batool Akhlaghinia*[a]

*Department of Chemistry, Faculty of Science, Ferdowsi University of Mashhad, Mashhad 9177948974, Iran

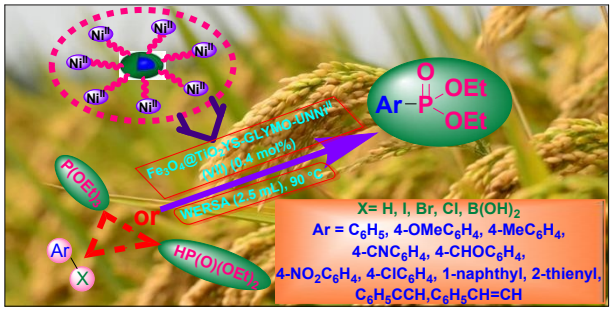

An efficient, versatile and novel method for C-P cross-coupling reaction with high yield of products using $Fe_3O_4@TiO_2$YS-GLYMO-UNNi^{II} as a magnetic nanostructured catalyst in the presence of WERSA was reported.